Temperature and Modulation Characteristics of Resonant-Cavity Light-Emitting Diodes

E. Fred Schubert, *Senior Member, IEEE,* N. E. J. Hunt, Roger J. Malik, *Senior Member, IEEE,* Miroslav Micovic, and David L. Miller, *Member, IEEE*

***Abstract*—Resonant-cavity light-emitting diodes (RCLED) are novel, high-efficiency light-emitting diodes which employ optical microcavities. These diodes have higher intensities and higher spectral purity as compared to conventional LED's. Analytical formulas are derived for the enhancement of the spontaneous emission along the optical axis of the cavity. The design rules for high-efficiency operation of RCLED's are established. The temperature dependence of the emission intensity is analyzed in the range 20–80° and it is described by an exponential dependence with a characteristic temperature of 112 K. The modulation characteristics of RCLED's exhibit 3 dB frequencies of 580 MHz. Eye diagrams at transmission rates of 622 Mb/s are wide open indicating the suitability of RCLED's for high-speed data transmission.**

I. Introduction

THE spontaneous emission of an optically active material can be changed by placing the material inside a microcavity whose fundamental optical mode is resonant with the natural emission wavelength of the optically active material. Such cavity structures were first proposed by Purcel [1] for emission frequencies in the microwave regime. The optically active materials that were used in microcavity structures include dyes [2], rare-earth elements [3], semiconductors [4], and polymers [5]. The changes in spontaneous emission characteristics found in microcavity structures include the spontaneous emission lifetime [6], the spectral purity [7], and the intensity of the emission along the optical axis of the microcavity [8]–[11].

The modification of the spontaneous emission characteristics of microcavity structures can be used in light-emitting diodes (LED's) to enhance their optical properties. Such resonant-cavity light-emitting structures were first proposed and demonstrated in 1992 [12]. The structure of a GaAs-based RCLED emitting through the substrate is shown in Fig. 1. The cavity of the RCLED is formed by an epitaxially grown distributed Bragg reflector (DBR) and an evaporated silver (Ag) reflector which also serves as a nonalloyed ohmic contact to the top p^+-doped semiconductor layer. The DBR is designed to have a lower reflectivity than the Ag reflector in order to couple the light out of the cavity through the GaAs substrate. The GaInAs quantum well active region has an emission wavelength of 900–950 nm, where the GaAs substrate is transparent. Most of the light emitted by the active region exits the semiconductor through the GaAs substrate which is coated by a ZrO_2 antireflection film. Further details of the device structure will be given below.

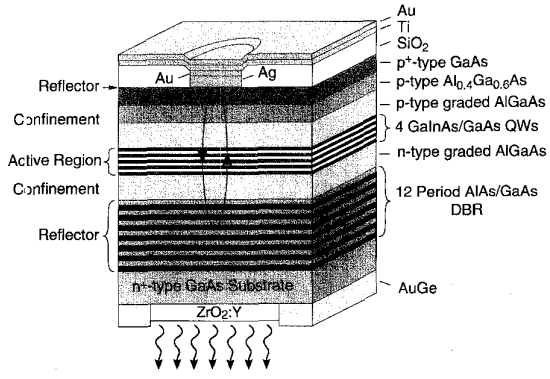

Fig. 1. Structure of a substrate-emitting GaAs-based resonant-cavity light-emitting diode (RCLED) emitting at 930 nm.

Light-emitting diodes have many advantages over semiconductor lasers including: i) higher reliability, ii) lower cost, and iii) simplicity of fabrication. These advantages make LED's the devices of choice for short and medium distance ($\leq$5 km), medium bit-rate ($\leq$1 Gb/s) optical fiber communication systems.

We first discuss the physics causing the changes of the spontaneous emission from an optically active medium located inside a microcavity and we will derive analytical formulas for the emission enhancement. The spontaneous radiative transition rate in an optically active, homogeneous medium is given by [13]

$$W_{spont} = \tau_{spont}^{-1} = \int_0^\infty W_{spont}^{(\ell)} \rho(\nu_\ell)\, d\nu_\ell \qquad (1)$$

where $W_{spont}^{(\ell)}$ is the spontaneous transition rate into the optical mode ℓ, and $\rho(\nu_\ell)$ is the optical mode density. Assuming that the optical medium is homogeneous, the spontaneous emission lifetime, τ_{spont}, is the inverse of the spontaneous emission rate. However, if the optical mode density in the

Manuscript received June 20, 1995; revised April 4, 1996. M. Micovic and D. L. Miller were supported in part by National Science Foundation under Grant ECS-9202642.

E. F. Schubert was with AT&T Bell Laboratories, Murray Hill, NJ 07974 USA. He is now with the Center for Photonics Research, Department of Electrical and Computer Engineering, Boston University, Boston, MA 02215 USA.

N. E. J. Hunt was with AT&T Bell Laboratories, Murray Hill, NJ 07974 USA. He is now with Mitra Imaging, Inc., Waterloo, Ont., Canada.

R. J. Malik was with AT&T Bell Laboratories, Murray Hill, NJ 07974 USA. He is now with Lucent Technologies, Bell Laboratories, Murray Hill, NJ 07974 USA.

M. Micovic and D. L. Miller are with the Department of Electrical Engineering, Pennsylvania State University, University Park, PA 16802 USA.

Publisher Item Identifier S 0733-8724(96)05444-8.

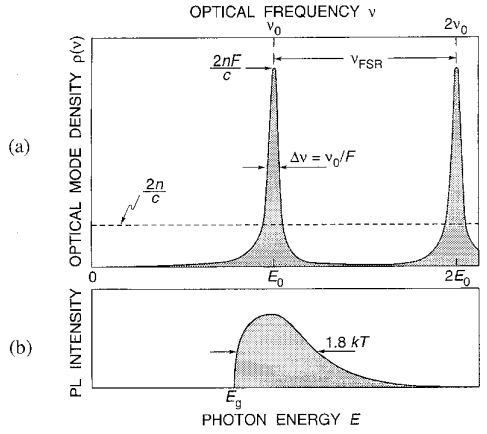

Fig. 2. (a) Optical mode density of a one-dimensional planar microcavity (solid line) and of a homogeneous one-dimensional space. (b) Theoretical shape of the luminescence spectrum of bulk semiconductors.

device depends on the spatial direction, as in the case of a cavity structure, then the emission rate given in (1) depends on the direction. Equation (1) can be applied to some small range of solid angle along a certain direction, for example the direction perpendicular to the reflectors of a Fabry–Perot cavity. The spontaneous emission rate into the optical mode ℓ, $W_{spont}^{(\ell)}$, contains the dipole matrix element of the two electronic states involved in the transition [13]. Thus, $W_{spont}^{(\ell)}$ will not be changed by placing the optically active medium inside an optical cavity. However, the optical mode density, $\rho(\nu_\ell)$, is strongly modified by the cavity.

We next compare the optical mode density in free space to the optical mode density in a microcavity. For simplicity, we restrict our consideration to the one-dimensional case, i.e., to the case of a coplanar Fabry–Perot microcavity. Furthermore, we restrict our consideration to the optical emission along the optical axis of the cavity. In a one-dimensional (1-D) homogeneous medium, the density of optical modes per unit length per unit frequency is given by

$$\rho(\nu) = \frac{2n}{c} \tag{2}$$

where n is the refractive index of the medium. Equation (2) can be derived using a similar formalism used for the derivation of the mode density in free space [13]. Equation (2) shows that the one-dimensional optical mode density is a constant, as shown in Fig. 2(a).

In planar microcavities, the optical modes are discrete and the frequency of these modes are integer multiples of the fundamental mode frequency. The fundamental mode is the optical mode with the lowest frequency, ν_0. For a cavity with two metallic reflectors (no distributed reflectors) and a zero or π phase shift of the optical wave upon reflection, the fundamental frequency is given by $\nu_0 = c/2nL_c$ where c is the velocity of light in vacuum and L_c is the length of the cavity. If the cavity length L_c equals one or a few multiples of one half of the emission wavelength of the optically active medium, the cavity is termed a *resonant microcavity*.

The optical mode density of a planar microcavity is schematically shown in Fig. 2(a). The fundamental and first excited mode occurs at the frequency ν_0 and $2\nu_0$, respectively. The spectral width of the optical modes can be derived from the photon lifetime in the cavity and the Heisenberg uncertainty principle. The spectral width of an optical mode, $\Delta\nu$, is given by

$$\Delta\nu = \frac{\nu_{\mathrm{FSR}}}{F} = \frac{\nu_0}{F} \tag{3}$$

where ν_{FSR} is the *free spectral range* of the Fabry–Perot cavity as shown in Fig. 2, and F is the finesse of the cavity. Equivalently, the spectral width of the mode can be expressed as

$$\frac{\nu}{\Delta\nu} = \frac{\lambda}{\Delta\lambda} = Q \tag{4}$$

where Q is the *cavity quality factor*. The finesse of a cavity is given by

$$F = \frac{\pi(R_1 R_2)^{1/4}}{1 - \sqrt{R_1 R_2}} \tag{5}$$

where R_1 and R_2 are the reflectivities of the two reflectors forming the cavity. The cavity Q is related to the finesse by

$$Q = \frac{2L_c}{\lambda} F \tag{6}$$

where L_c is the cavity length and λ is the wavelength of the cavity mode of interest. The peaks of the optical mode density in a cavity occur at the frequencies ν_0, $2\nu_0$, $3\nu_0$, $\cdots$, as shown in Fig. 2.

We next determine the peak value of the optical mode density at the frequency of the fundamental mode, i.e., $\rho(\nu_0)$. The peak mode density can be derived by integration of the mode density in the vicinity of ν_0 over frequency and the cavity length L_c, which yields the number of optical modes. Integration over the fundamental mode of the cavity yields

$$\int_0^{L_c} \int_{\nu_0 - \nu_0/2}^{\nu_0 + \nu_0/2} \rho(\nu)\, dL\, d\nu \approx \rho(\nu_0)\, \frac{\nu_0}{F}\, L_c = 1. \tag{7}$$

The result of (7) yields *unity*, because the integration is carried out over *one* optical mode. The peak optical mode density is then given by

$$\rho(\nu_0) = \frac{2nF}{c} \tag{8}$$

Comparison of (2) with (8) shows a significant enhancement of the emission rate at the resonance frequency of the cavity where the optical mode density of a 1-D microcavity is a factor of F larger than that of a 1-D homogeneous medium. Because the emission rate at a given frequency is directly proportional to the optical mode density [see (1)], the emission rate at the resonance wavelength will be enhanced by the finesse of the cavity. Thus the emission rate enhancement at the resonance, G_e, is given by

$$G_e \approx F = \frac{\pi(R_1 R_2)^{1/4}}{1 - \sqrt{R_1 R_2}}. \tag{9a}$$

This equation represents the *average* emission rate enhancement out of *both* reflectors. To find the enhancement out a

single direction, we multiply the enhancement given by (9a) by the fraction of the light exiting the mirror with reflectivity R_1 divided by the average loss of the two mirrors for one round trip in the cavity. For large R_1 and R_2, this gives for the enhancement of the emission exiting R_1

$$G_e \approx \frac{2(1-R_1)}{2-R_1-R_2}F \approx \frac{1-R_1}{1-\sqrt{R_1R_2}}F = \frac{\pi(R_1R_2)^{1/4}(1-R_1)}{(1-\sqrt{R_1R_2})^2}. \quad (9b)$$

This equation represents the emission rate enhancement out of a *single* reflector with reflectivity R_1. The result of (9a) and (9b) can be also obtained by quantum-theoretical calculations [14]. However, (9a) and (9b) do not take into account the standing wave effect, that is, the distribution of the optically active material within the cavity.

The exact expression for G_e valid for all combinations of reflectivities R_1 and R_2 is given by [6]

$$G_e = \frac{\xi}{2}\frac{(1+\sqrt{R_2})^2(1-R_1)}{(1-\sqrt{R_1R_2})^2}\frac{\tau_{cav}}{\tau} \quad (10)$$

where R_1 is the reflectivity of the light-exit mirror and therefore $R_1 < R_2$. Equation (10) takes into account the standing wave effect, which provides an additional enhancement if the optically active medium is located at the antinode of the standing optical wave of the cavity. The antinode enhancement factor ξ has a value of 2, if the active region is located exactly at an antinode of the standing wave inside the cavity. The value of ξ is unity, if the active region is smeared out over many periods of the standing wave. Finally $\xi = 0$, if the active material is located at a node. Equation (10) also takes into account changes in the spontaneous emission lifetime. For planar microcavities, the ratio of the spontaneous lifetime with cavity, τ_{cav}, and the lifetime without cavity, τ, is about $\tau_{cav}/\tau \approx 0.9$ [6]. Note that (10) gives an enhancement factor which is by $(1+\sqrt{R_2})^2/[\pi(R_1R_2)^{1/4}] \approx (4/\pi)$ *higher* than that given in (9b). This discrepancy is due to the approximation made in (7).

The total enhancement integrated over all wavelengths, rather than the enhancement at the resonance wavelength, is relevant for many practical devices. Exactly on resonance, the emission is enhanced along the axis of the cavity. However, sufficiently far off resonance, the emission is suppressed. Because the natural emission spectrum of the active medium (without cavity) may be much broader than the cavity resonance, it is, *a priori,* not clear if the integrated emission is enhanced at all. To calculate the wavelength-integrated enhancement, the spectral width of the cavity resonance and the spectral width of the natural emission spectrum must be determined. The former can be calculated from the uncertainty relation and it is given by (3).

The theoretical width of the emission spectrum of bulk semiconductors is $1.8kT$ [15], where k is the Boltzmann constant and T is the absolute temperature. At room temperature, $1.8kT$ corresponds to an emission linewidth of $\Delta\lambda_n = 31$ nm assuming an emission wavelength of 900 nm. For a cavity resonance width of 5–10 nm, one part of the spectrum is strongly enhanced, whereas the rest of the spectrum is suppressed. The integrated enhancement ratio (or suppression ratio) can be calculated analytically by assuming a Gaussian natural emission spectrum which is, at room temperature, much larger than the width of the cavity resonance. The integrated enhancement ratio (or suppression ratio) is then given by [8]

$$G_{int} = G_e\sqrt{\pi \ln 2}\,\frac{\Delta\lambda}{\Delta\lambda_n}. \quad (11)$$

The value of G_{int} can be quite different for different types of optically active materials. Narrow atomic emission spectra can be enhanced by several orders of magnitude [4]. On the other hand, materials having broad emission spectra such as dyes or polymers [2] may not exhibit any integrated enhancement at all.

We next calculate the wavelength-integrated enhancement for the RCLED structure discussed in this publication by using (10) and (11). With the reflectivities $R_1 = 90\%$ and $R_2 = 97\%$, an antinode enhancement factor of $\xi = 1.5$ and $\tau_{cav}/\tau \approx 1$, one obtains a peak enhancement factor of $G_e = 68$ by using (10), and a finesse of $F = 46$ by using (5). Insertion of this value into (11), using a cavity resonance bandwidth of $\Delta\lambda = 6.5$ nm [8], and the theoretical 300 K natural emission linewidth of $\Delta\lambda = 31$ nm, one obtains an integrated enhancement factor of $G_{\rm int} = 21$. Experimental enhancement factors of five have been demonstrated [8] which is lower than the theoretical value. The discrepancy is in part due to a broader natural emission linewidth which exceeds the theoretical value of $1.8kT$.

The spontaneous emission spectrum of a bulk semiconductor is shown in Fig. 2(b). For optimum performance of RCLED's, the cavity must be in resonance with the natural emission spectrum, as shown in Fig. 2. Note that additional broadening mechanisms, such as alloy broadening will broaden the natural emission spectrum over its theoretical value of $1.8kT$. Quantum-well structures have an inherently narrower spectrum ($0.7kT$), due to the step-function-like density of states. Low temperatures and excitonic effects can further narrow the natural emission linewidth. Thus, even higher enhancements are expected for low temperatures and quantum well active regions.

Resonant-cavity LED's have been reported for emission wavelengths in the 850–950 nm range [7], [8], [12], [16], and in the visible spectral range [17], [18]. For the visible RCLED's, the emission band was 4.8 nm wide with a peak emission at 670 nm. AlInP/(AlGa)InP distributed Bragg reflectors (DBR) were used as bottom and top reflectors [17], [18].

II. Experimental

The epitaxial layers used in this study were grown by molecular-beam epitaxy on (001) oriented N^+-type GaAs substrates. The epitaxial layer sequence consist of a 9 pair AlAs (783 Å)/GaAs (655 Å) DBR doped at $N_D = 3 \times 10^{18}$ cm^{-3} followed by the lower confinement region consisting

of $Al_{0.40}Ga_{0.60}As$ linearly graded to GaAs over a thickness of 960 Å. The bottom half of the graded confinement region is doped at $N_D = 1 \times 10^{18}$ cm^{-3}. The active region consists of a 100 Å thick undoped GaAs layer followed by 3 undoped $Ga_{0.86}In_{0.14}As$ (80 Å) quantum wells separated by 100 Å undoped GaAs layer. The last GaInAs quantum well is clad by a 100 Å thick undoped GaAs layer. The upper confinement region is linearly graded from GaAs to $Al_{0.40}Ga_{0.60}As$ over 1000 Å. The top half of the upper confinement region is p-type doped at $N_A = 5 \times 10^{17}$ cm^{-3}. The p-type confinement region is clad by 250 Å $Al_{0.40}Ga_{0.60}As$ ($N_A = 1 \times 10^{19}$ cm^{-3}). A 300 Å thick GaAs contact layer ($N_A = 3 \times 10^{19}$ cm^{-3}) completes the epitaxial growth.

After epitaxial growth, the wafers are mapped by photoluminescence and reflectivity measurements. The wafers are processed by first depositing borosilica glass on the p-side of the wafer. After thinning the wafer to 125 μm, cubic zirconia is deposited on the substrate side of the wafer as an antireflection coating. The n-type metallization consists of AuGe/Ni/Au annealed at 380 °C for 30 sec. Circular 175 μm diameter cubic zirconia windows serve as light-exit regions on the substrate side. The p-type contact consists of 2000 Å Ag followed by 500 Å Au, and a Ti/Au metallization for wire bonding. The Ag serves as a nonalloyed p-type ohmic contact as well as a reflector.

Room-temperature electroluminescence measurements were carried out using phase-sensitive "lock-in" detection and a Si photodetector. Optical power measurements were performed by using a HP 8153A optical power meter with a Si-detector head. The light collection solid angle of the power measurements was $\pm 10° \times \pm 10°$ about the optical axis of the cavity. For the high-speed measurements, the light emanating from RCLED's was butt coupled into a 62.5 μm core diameter step-index multimode optical fiber. The modulated light was detected by a high-speed optoelectronic converter (BCP, Model 310) and a Tektronix sampling oscilloscope (Tek 7704A). The devices were modulated with a pulse generator HP 8131A and an Anritsu bit pattern generator for "eye-diagram" measurements.

III. RCLED Design Parameters

We next summarize several design rules for RCLED's. This summary will also provide further insight in the fundamental operating principles of RCLED's and the differences of these devices from vertical-cavity surface-emitting lasers (VCSEL's). The first design criterion for RCLED's is that the reflectivity of the light-exit reflector, R_1, should be much lower than the reflectivity of the back reflector, i.e.,

$$R_1 \ll R_2. \tag{12}$$

This condition implies that light exits the device mainly through the reflector with reflectivity R_1. This condition is required for communication LED applications (where all light should be emitted into the core of a multimode fiber) as well as for display LED's (where all light should be emitted to the observer). For the RCLED's discussed here, the back reflector is a silver mirror. On GaAs, silver reflectors have typical reflectivities of 96–97%. Thus, the DBR front mirror (see Fig. 1) is designed to have a reflectivity less than 96%.

The second design criterion calls for a short cavity length L_c. In order to derive this criterion, the integrated enhancement is rewritten by insertion of (4), (6), and (10) into (11). One obtains

$$G_{int} = \xi \sqrt{\frac{\ln 2}{\pi}} \frac{\lambda}{L_c} \frac{\lambda_0}{\Delta\lambda_n} \frac{2(1-R_1)}{2-R_1-R_2} \frac{\tau_{cav}}{\tau} \tag{13}$$

where λ is the operating wavelength in the cavity and λ_0 is the operating wavelength in air. Assuming that the operating wavelength λ_0 and the natural linewidth of the active medium (in air), $\Delta\lambda_n$, are given quantities, (13) shows that a short cavity length L_c maximizes the integrated intensity. The shortest possible cavity length is obtained, if the fundamental mode of the cavity is in resonance with the emission from the active medium. The cavity length is also reduced by using a DBR with a short penetration depth, i.e., a DBR consisting of two materials with a large difference in the refractive index. Note that (10) also shows that the active medium should be placed in the antinode position of the optical standing wave in the cavity which yields $\xi = 2$.

The third design criterion discussed here is the minimization of self-absorption in the active region. This criterion can be stated as follows: the reabsorption probability of photons emitted from the active region into the cavity mode should be much smaller than the escape probability of photons through one of the reflectors. Assuming $R_2 \cong 1$, this criterion can be written as

$$2\xi\alpha\ell \ll (1-R_1) \tag{14}$$

where α and ℓ are the absorption coefficient and the length of the active area, respectively. If the criterion of (14) were not fulfilled, photons in the fundamental cavity mode would be reabsorbed by the active region. Subsequently, re-emission could occur to the side, i.e., not into the cavity mode. Thus, if the condition of (14) is not fulfilled, the emission intensity of a microcavity is lowered rather than enhanced.

Whereas the condition of (14) is fulfilled in RCLED's, it is clearly not fulfilled in vertical-cavity surface-emitting lasers (VCSEL's). We have therefore compared the spontaneous emission intensities of RCLED's and VCSEL's. In this comparison, the VCSEL was pumped below the threshold current. The spontaneous emission spectra of an RCLED and a VCSEL driven by an injection current of 2 mA are shown in Fig. 3. The threshold current of the VCSEL is 7 mA. The VCSEL has an AlGaAs/GaAs quantum-well active region emitting at 850 nm. Both reflectors of the VCSEL are AlGaAs/AlAs DBR's. Fig. 3 reveals that the emission intensity of the VCSEL in the *spontaneous* regime is more than a factor of ten lower than the emission intensity from the RCLED. VCSEL's do not fulfill (14): Because the magnitude of the maximum gain in semiconductors is always lower than the magnitude of the absorption coefficient in an unpumped semiconductor ($|g| < |\alpha|$), VCSEL's could not lase if the condition of (14) were met. Thus, the spontaneous emission intensity in VCSEL's is low and must be low in order to enable the device to lase.

Fig. 3 also reveals that the emission spectral linewidth of VCSEL's is narrower than that of RCLED's. The higher

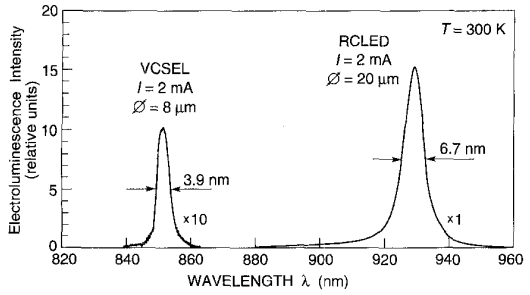

Fig. 3. Spontaneous electroluminescence spectrum of a vertical-cavity surface-emitting laser (VCSEL) emitting at 850 nm and of a resonant-cavity light-emitting diode (RCLED) emitting at 930 nm. The drive currents for both devices are 2 mA. The VCSEL spectrum is multiplied by a factor of ten. The threshold current of the VCSEL is 7 mA.

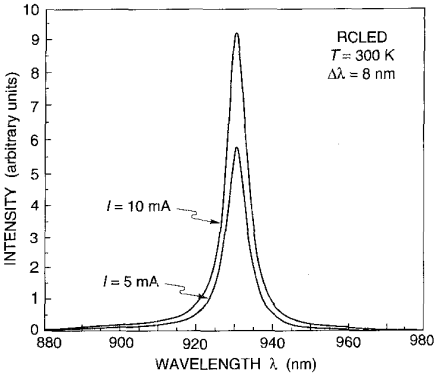

Fig. 4. Electroluminescence spectrum of an RCLED emitting at 930 nm at drive currents of 5 and 10 mA.

spectral purity is due to the higher values of R_1 and R_2 which in turn are required in VCSEL's to enable the devices to lase.

The fulfillment of (14) by RCLED's also implies that these devices cannot lase. As stated above, it is always ($|g| < |\alpha|$). As a consequence, the mirror loss $(1 - R_1)$ is always larger than the maximum achievable round-trip gain $(2\xi g\ell)$. The fundamental inability of RCLED's to lase has been experimentally verified by pulsed injecting currents in excess of 1000 mA without evidence for lasing. The spectral stability of RCLED's is demonstrated in Fig. 4 which shows the electroluminescence spectra for injection currents of 5 and 10 mA. The spectral shape of the emission is very stable and nearly identical for the two injection currents. The stability of the emission spectrum is found for direct currents ranging from 0.5–50 mA as well as for pulsed currents.

The arguments used above imply that the *spontaneous* emission into the fundamental cavity mode in VCSEL structures is very low due to reabsorption of photons by the active region. A reduction of the threshold current by increasing the reflectivity will be accompanied by a further decrease of the *spontaneous* emission below the threshold current. We therefore conclude that the so-called zero-threshold laser [19], [20] cannot be realized by planar microcavity structures.

IV. Temperature-Dependence of RCLED Characteristics

The emission intensity of RCLED's depends, as in conventional LED's, on the temperature. Several materials parameters depend on temperature including the energy gap of the semiconductor active region. The gap energy of semiconductors decreases with increasing temperature and the temperature dependence of the energy gap can be calculated by

$$E_g = E_g(0\,\mathrm{K}) - \frac{\alpha T^2}{T + \beta}. \tag{15}$$

For GaAs, the parameters are given by $E_g(0\,\mathrm{K}) = 1.519$ eV, $\alpha = 5.41 \times 10^{-4}$ eV/K and $\beta = 204$ K. In the temperature range $20°\mathrm{C} \leq T \leq 100\,°\mathrm{C}$, the dependence of E_g on T is approximately linear. Thus, the luminescence signal of the active area shifts to longer wavelengths as the temperature is increased.

Second, the resonance of the Fabry–Perot cavity shifts with temperature, due to i) the dependence of the refractive index on temperature, and ii) the change of the layer thicknesses caused by thermal expansion. Generally, the modes of semiconductor Fabry–Perot cavities shift to longer wavelengths as the temperature is increased. However, the shift of the cavity resonance mode is much smaller than the shift of the peak wavelength emitted from the active semiconductor material [21].

Assume that the peak of the natural emission spectrum and the cavity resonance are matched at room temperature. Thus, considering the two different temperature dependences of the gap energy and the cavity mode, the natural emission spectrum and the cavity mode will be off resonance at temperatures other than room temperature. A decrease in the optical intensity is therefore expected for $T > 300$ K.

A decrease of the RCLED optical output power is also expected due to a decreasing radiative efficiency at higher temperatures. This well-known decrease is due to the temperature dependence of nonradiative Shockley–Read recombination processes and due to the temperature dependence of nonradiative Auger recombination processes.

The intensity-versus-current characteristics of an RCLED is shown in Fig. 5 for temperatures ranging from 21–80 °C. At room temperature, the emission wavelength of the device is 930 nm and the peak of the natural emission spectrum is matched to the Fabry–Perot resonance. The light output shown in Fig. 5 decreases as the device is heated to 80 °C. At this temperature, the light output is 62% of the room-temperature value.

Also shown in Fig. 5 is the calculated intensity of the *perfect isotropic emitter*. This hypothetical planar device is assumed to have a 100% internal quantum efficiency, and an antireflection coating providing zero reflectivity at all wavelengths. The emission pattern within the active material of this hypothetical device is assumed to be isotropic. The light intensity emitted by the ideal isotropic emitter has been calculated for emission normal to the planar semiconductor surface [8]. Fig. 5 reveals that the measured intensity of the RCLED exceeds the calculated emission intensity of the ideal isotropic emitter.

The intensity of the RCLED at 7.5 mA is shown in Fig. 6 as a function of temperature. The temperature dependence of the intensity can be expressed by the exponential dependence

$$I = I_0 e^{-T/T_1} \tag{16}$$

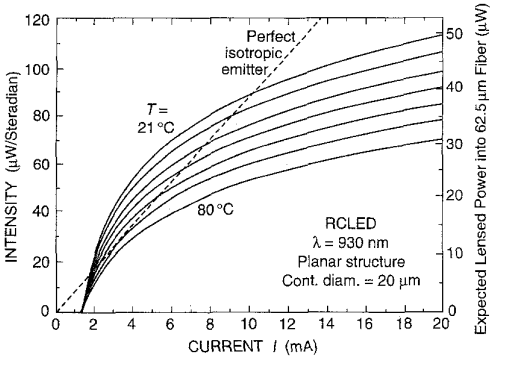

Fig. 5. Intensity-versus-current (LI) for an RCLED emitting at 930 nm for different temperatures. The traces are measured at the temperatures 21, 30, 40, 50, 60, 70, and 80 °C. Also shown in the theoretical LI curve of the "ideal isotropic emitter."

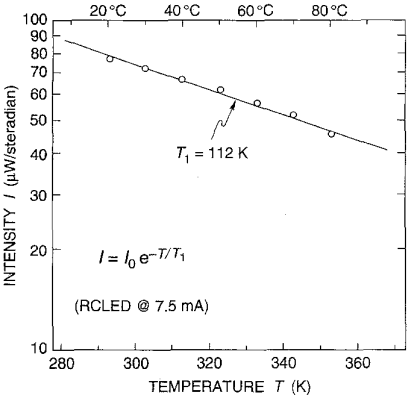

Fig. 6. Electroluminescence intensity of an RCLED at a drive current of 7.5 mA as a function of temperature. The temperature dependence is described by an exponential function with a characteristic temperature of $T_1 = 112$ K.

where I_0 is a reference intensity. The dependence given in (16) is frequently called the T_1-law, in analogy to the T_0-law in lasers. The semilogarithmic plot of the intensity versus temperature allows the evaluation of the characteristic temperature T_1. Evaluation of the data shown in Fig. 6 yields a characteristic temperature of $T_1 = 112$ K.

Note that the GaInAs/GaAs quantum wells are relatively shallow. We expect that by using the deeper GaInAs/AlGaAs quantum wells, the free-carrier confinement and the values for T_1 can be further improved.

The current-voltage curves of the RCLED for the two temperatures 20 and 80 °C are shown in Fig. 7. The threshold voltage decreases by a small amount (≅30 mV) at 80 °C when compared to the 20 °C value. This decrease is consistent with the decrease of the gap energy.

The current-voltage characteristic displays a leakage current of approximately 1.4 mA at the threshold voltage (1.3 V). The device structure is planar and has no mesa. We assume that the leakage current is due to current flow from the top contact through the top p-layer to the chip edge. At the chip edge, the structure of the semiconductor is strongly perturbed which gives rise to the ohmic leakage component displayed in the current-voltage curve. The leakage current is also evidenced

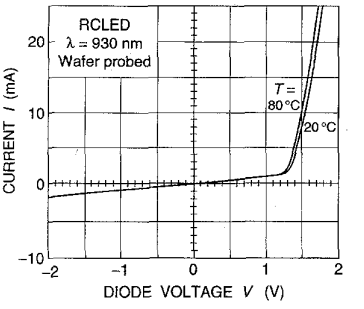

Fig. 7. Current-voltage characteristics of an RCLED at room temperature and at 80 °C.

by the "foot" in the intensity-versus-current curves shown in Fig. 5. For voltages larger than 1.3 V, the pn-junction below the p-type contact "turns on" and light is emitted from the device. This interpretation is supported by Fig. 5 which shows that no light is emitted for currents below 1.3 mA. The magnitude of the leakage current can be strongly reduced by mesa etching [8].

V. High-Speed Characteristics

Application of RCLED's in optical communication systems requires that the diode can be modulated at high speed. The modulation is generally achieved by a pulsed injection current. A fundamental limit of the modulation speed is given by the spontaneous recombination lifetime of free carriers. For III–V semiconductors, this spontaneous lifetime is on the order of 1 ns, which implies a maximum modulation rate of approximately 1 Gb/s.

In RCLED's, the spontaneous lifetime can be shorter than the bulk lifetime due to the resonant-cavity effect. However, the lifetime is the inverse emission rate integrated over all spatial directions. Whereas the emission rate along the cavity axis is strongly enhanced, the emission rates along the other directions are not altered significantly. Therefore, the spontaneous lifetime in RCLED's is reduced by about 10% [22]. The RCLED's discussed here employ quantum well active regions. The lifetime of quantum-well structures is reduced as compared to bulk semiconductors due to the larger overlap of the electron and hole wave function in quantum well structures. It is consequently expected that RCLED's can be modulated at higher speeds than conventional bulk LED's.

The rise time and the fall time of the optical signal of an RCLED is shown in Fig. 8(a) and (b), respectively. The times include the time constant of the pulse generator, the RCLED, the detector, detector amplifier circuit, and the oscilloscope. However, the time constant of the RCLED is the longest and hence the dominant time constant. Thus, the time constants shown in Fig. 8 are *upper limits* to the true time constants of the RCLED.

Fig. 8 reveals that the rise time and fall time of the RCLED are 2.4 ns and 1.1 ns, respectively. The rise time is more than twice as long as the fall time of the RCLED. The bias values for the "on" and "off" state of the RCLED are 1.4 V and 0 V, respectively. We explain the strong asymmetry of the rise and fall time as follows. Upon application of the "on"

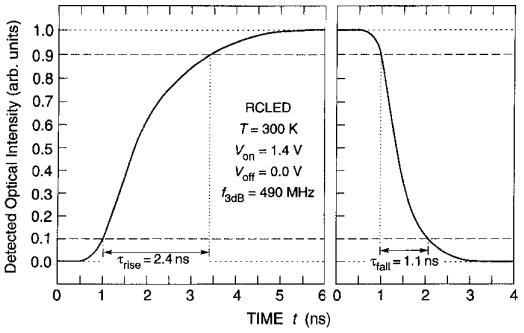

Fig. 8. Detected optical signal emitted by an RCLED driven by a square-shaped pulse.

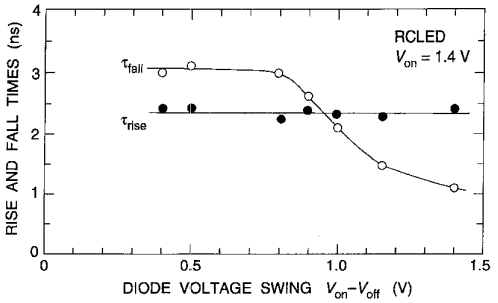

Fig. 9. Rise and fall times of an RCLED as a function of the voltage swing displayed on the pulse generator.

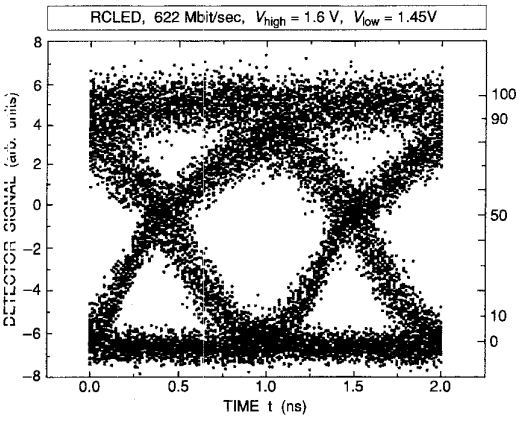

Fig. 10. Eye diagram of the detected optical signal emitted by an RCLED. The data rate is 622 Mb/s.

voltage to the RCLED, free carriers will accumulate inside the quantum well. The steady-state emission intensity is achieved after a time on the order of the spontaneous lifetime. We next consider the transition to the "off" state of the diode. When the injection current is reduced to zero, and the free carriers in the quantum well would recombine radiatively, it would again take the spontaneous recombination lifetime until the emission intensity has dropped to the $1/e$ value. However, at zero bias (which is the "off" value of the voltage) the band diagram of the active region is highly sloped due to the built-in electric field of the pn junction. As a result, the free carriers are swept out of the quantum wells into the neutral regions of the semiconductor. This sweep-out time can be much shorter than the spontaneous lifetime. Thus, the fall time is determined not by the spontaneous recombination lifetime but by the shorter sweep-out time. Considering the magnitude of the built-in electric field and the carrier mobility, we estimate the sweep-out time to be in the ps range.

To further clarify the origin of the difference in rise and fall time, the bias of the "off" state has been varied. The results of this measurement are shown in Fig. 9. The fall time displays a pronounced dependence on the voltage swing. The fall time is shortest for the largest voltage swing, i.e., if the "off" state voltages is zero. This dependence is consistent with the sweep-out model outlined above. The dependence of the fall time on the bias cannot be explained by a simple RC time constant where R and C are independent of voltage. Such an RC limitation would not exhibit the voltage dependence shown in Fig. 9.

The 3 dB frequency of the RCLED's has been determined by measuring the frequency at which the detector signal decreases to one half of the low-frequency value. A small nonlinearity of the detector was corrected for in the measurement. A 3 dB frequency of 490 MHz has been measured for the RCLED. The rise and fall times of this device are shown in Fig. 8. Comparison of the 3 dB frequencies for different RCLED structures revealed that the highest 3 dB frequencies were attained with devices having a thick SiO_2 isolation layer on the p-type side of the device (see Fig. 1 for illustration) and a small area of the bonding pad on the p-type side of the device. We expect that the 3 dB frequency can be further enhanced by reducing the parasitic bond pad capacitance.

The 3 dB frequency can be also increased by *pulse-shaping*. The square-wave-shaped drive voltage can be pulse-shaped by placing a parallel RC circuit in series with the diode. The R value of this circuit is chosen to equal the resistance of the diode. Fig. 7 reveals that the diode resistance is about 20 Ω at a drive current of 10 mA. The capacitance of the circuit was chosen to be 100 pF. The RC time constant of this circuit is then $\tau = RC = 2.5$ ns which coincides with the RCLED rise time. By using the RC circuit in series with the RCLED, the 3 dB frequency of the RCLED increased to 580 MHz.

Eye diagram measurements were performed to assess the suitability of RCLED's for high-speed data transmission. The eye diagram at a data rate of 622 Mb/s is shown in Fig. 10. This data rate is used in the well-known "synchronous optical network" (SONET) standard. The "eye" shown in Fig. 10 is wide open indicating that a low bit error rate data transmission is possible at that frequency by using RCLED's. The "on" and "off" pulse-generator voltages of the diode were 1.4 and 1.1 V, respectively. A pulse shaping RC circuit with R = 20 Ω and C = 100 pF was used for the measurement. We expect that minimizing parasitic elements (e.g., bond pad capacitance) and by the employment of a simple pulse shaping circuit, data transmission rates of 1 Gb/s will be attainable.

This bias values for the "on" and "off" state of the RCLED used in the eye diagram measurements are 1.4 and 1.1 V, respectively. These values were read off the display of the pulse generator. The display voltage applies to loads of 50 Ω.

The differential resistance of the diode in the "on" state is 25 Ω. A 25 Ω resistor was put in series to the diode in order to match the impedance to the 50 Ω coaxial line. That is, for voltages exceeding the diode threshold voltage, the load has a differential resistance of $dV/dI = 50\,\Omega$. We have calculated the true voltage at the diode to be 1.6 and 1.45 V for a pulse generator display voltage of 1.4 and 1.1 V, respectively. Note that for loads with dc resistances $V/I > 50\,\Omega$, the voltages at the load exceed the voltage displayed by the pulse generator.

We finally note that the spectral linewidth of the RCLED reduces the chromatic dispersion of silica fibers at the operating wavelength of 930 nm. The reduced chromatic dispersion allows for either higher data rates or for longer transmission distances for stepped-index and graded-index multimode fibers [23].

VI. Conclusions

In conclusion, the fundamental characteristics of RCLED's have been analyzed. The optical mode density in a one-dimensional cavity is strongly modified when compared to the one-dimensional mode density in homogeneous space. As a consequence, the optical characteristics of RCLED's are changed including the spectral purity, far field, brightness, and spontaneous recombination rate. Analytical formulas were derived for the on-axis spectral enhancement and the wavelength-integrated enhancement. The design criteria for optimum performance of RCLED's were summarized and the differences between RCLED's and VCSEL's were analyzed. The spontaneous emission intensity of an RCLED was shown to be more than one order of magnitude higher than that of a VCSEL at the same injection current. The temperature dependence of the light output of RCLED's was studied. The temperature dependence is expressed in terms of a T_1-law where the characteristic temperature T_1 has a value of 112 K. High-speed measurements on RCLED's reveal that the rise time is determined by the spontaneous emission lifetime of carriers in the quantum well. The shorter fall time is determined by the time required to sweep the carriers out of the quantum wells. This time is much shorter than the spontaneous recombination time. A 3 dB frequency of 580 MHz was demonstrated. High-speed measurements at 622 Mb/s reveal a wide open eye diagram demonstrating that high-speed data transmission capability of RCLED's.

References

[1] E. M. Purcell, *Phys. Rev.*, vol. 69, p. 681, 1946.
[2] F. de Martini, G. Innocenti, G. R. Jacobovitz, and P. Mataloni, *Phys. Rev. Lett.*, vol. 59, p. 2955, 1987, see also: M. Suzuki, H. Yokoyama, S. D. Brorson, and E. P. Ippen, *Appl. Phys. Lett.*, vol. 58, p. 998, 1991.
[3] E. F. Schubert, A. M. Vredenberg, N. E. J. Hunt, Y. H. Wong, P. C. Becker, J. M. Poate, D. C. Jacobson, L. C. Feldman, and G. J. Zydzik, *Appl. Phys. Lett.*, vol. 61, p. 1381, 1992.
[4] H. Yokoyama, K. Nishi, T. Anan, H. Yamada, S. D. Brorson, and E. P. Ippen, *Appl. Phys. Lett.*, vol. 57, p. 2814, 1990.
[5] A. Dodabalapur, L. J. Rothberg, and T. M. Miller, *Appl. Phys. Lett.*, vol. 65, p. 2308, 1994.
[6] A. M. Vredenberg, N. E. J. Hunt, E. F. Schubert, D. C. Jacobson, J. M. Poate, and G. J. Zydzik, *Phys. Rev. Lett.*, vol. 71, p. 517, 1993.
[7] N. E. J. Hunt, E. F. Schubert, R. A. Logan, and G. J. Zydzik, *Appl. Phys. Lett.*, vol. 61, p. 2287, 1992.
[8] E. F. Schubert, N. E. J. Hunt, M. Micovic, R. J. Malik, D. L. Sivco, A. Y. Cho, and G. J. Zydzik, *Science*, vol. 265, p. 943, 1994.
[9] J. Blondelle, H. De Neve, P. Demeester, P. Van Daele, G. Borghs, and R. Baets, *Electr. Lett.*, vol. 30, p. 1787, 1994.
[10] H. De Neve, J. Blondelle, R. Baets, P. Demeester, P. Van Daele, and G. Borghs, *IEEE Photon. Tech. Lett.*, vol. 7, p. 287, 1995.
[11] D. G. Deppe and C. Lei, *Appl. Phys. Lett.*, vol. 60, p. 527, 1992.
[12] E. F. Schubert, Y.-H. Wang, A. Y. Cho, L.-W. Tu, and G. J. Zydzik, *Appl. Phys. Lett.*, vol. 60, p. 921, 1992.
[13] See, for example, A. Yariv, *Theory and Applications of Quantum Mechanics*. New York: Wiley, 1982, p. 143.
[14] X.-P. Fend and K. Ujihara, *Phys. Rev.*, vol. A41, p. 2668, 1990.
[15] E. F. Schubert, *Doping in III–V Semiconductors*. Cambridge, England: Cambridge University Press, 1993, p. 512.
[16] D. L. Huffaker, C. C. Lin, J. Shin, and D. G. Deppe, *Appl. Phys. Lett.*, vol. 66, p. 3096, 1995.
[17] J. A. Lott, R. P. Schneider, Jr., J. C. Zolper, and K. J. Malloy, *IEEE Photon. Technol. Lett.*, vol. 5, p. 631, 1993.
[18] J. A. Lott, R. P. Schneider, Jr., G. A. Vawter, J. C. Zolper, and K. J. Malloy, *Electron. Lett.*, vol. 29, p. 328, 1993.
[19] T. Kobayashi, T. Segawa, A. Morimoto, and T. Sueta, in *43rd Fall Meeting Japanese Soc. Appl. Phys.*, Tokyo, Japan, Sept. 1982.
[20] H. Yokoyama, *Science*, vol. 256, p. 66, 1992.
[21] J. Talghader and J. S. Smith, in *Conf. Lasers and Electro-Optics*, Baltimore, MD, Paper CWF4, May 1995.
[22] A. M. Vredenberg, N. E. J. Hunt, E. F. Schubert, D. J. Jacobson, J. M. Poate, and C. J. Zydzik, *Phys. Rev. Lett.*, vol. 71, p. 517, 1993.
[23] N. E. J. Hunt, E. F. Schubert, R. F. Kopf, D. L. Sivco, A. Y. Cho, and C. J. Zydzik, *Appl. Phys. Lett.*, vol. 63, p. 2600, 1993.

E. Fred Schubert (S'80–M'85–SM'93) was born in Germany in 1956. He received the Dipl.-Ing. degree with honors from the University of Stuttgart, Germany in 1981. In the same year, he joined the Max Planck Institute of Solid State Research, Stuttgart, and received the Dr.-Ing. degree with honors from the University of Stuttgart in 1986.

As part of his graduate study, he worked on MBE growth and characterization of high-speed AlGaAs/GaAs Schottky gate field-effect transistors based on III-V semiconductors. During his thesis, he also developed the theory of luminescence line broadening in ternary and quaternary alloy semiconductors. In 1985, he joined AT&T Bell Laboratories, Holmdel, NJ, as a Postdoctoral Fellow working on the fabrication and characerization of III-V smeiconductor devices. From 1988 to 1995, he worked there as a Principal Investigator in the Physics Research Division. His research focused on electronic and optoelectronic heterostructure materials, devices, and systems. He made pioneering contributions to the doping of compound semiconductors, in particular to the development of delta doping. He invented a method by which the band discontinuities occurring at semiconductor heterojunctions can be eliminated, thereby reducing the heterojunction resistance. This method is now routinely used in heterojunction devices containing distributed Bragg reflectors. While at AT&T, he also pioneered the field of Er-doped microcavities and of resonant cavity light-emitting diodes (RCLED's) which use enhanced spontaneous emission for high brightness LED's. In 1995, he joined the Center for Photonics Research at Boston University and was appointed Full Professor in the Department of Electrical and Computer Engineering. He is responsible for the fabrication and testing of III-V semiconductor devices, in particular GaN-based photonic devices.

Dr. Schubert has published more than 120 research papers and review articles, contributed several chapters in books, and is the inventor of 25 U.S. patents and more than 40 foreign patents. He is the author of the book, *Doping in III-V Semiconductors*, (Cambridge University Press, 1993), for which he was awarded the 1994 Literature Price of the Verein Deutscher Elektrotechniker (VDE). He is editor of the book, *Delta Doping of Semiconductors*, (Cambridge University Press, 1996). He has served on several technical committees of conferences on compound semiconductor devices. He is a Senior Member of the IEEE, a member of the American Physical Society, the Optical Society of America, and a Fellow of the Bohemian Physical Society.

N. E. J. Hunt, photograph and biography not available at the time of publication.

Roger J. Malik (S'75–M'78–SM'90) was born in Queens, NY, on August 3, 1954. He received the B.E. degree, with high honors, in electrical engineering from the State University of New York at Stony Brook in 1976, and the M.S. and Ph.D. degrees in electrical engineering from Cornell University in 1978 and 1981, respectively.

From 1978 to 1982, he held the position of Research Physical Scientist at The U.S. Army Electronics Technology and Devices Laboratory, Fort Monmouth, NJ. His principal areas of research were in advanced III-V semiconductor device structures formed by molecular beam epitaxy (MBE). While at Fort Monmouth, he invented the planar doped barrier (PDB) concept which was the subject of his Ph.D. dissertation. In 1982, he joined AT&T Bell Laboratories as a Member of Technical Staff, where he is presently engaged in research on the MBE growth, fabrication, and characterization of III-V heterojunction bipolar transistors, lasers, and PDB diodes. He has authored or co-authored over 100 technical papers and over 100 talks at international conferences. He also has been awarded 16 U.S. patents.

Dr. Malik has received several awards for his work on planar doped barrier devices including the U.S. Army Special Act Award and the Paul A. Siple Award at the 1982 U.S. Army Science Conference. He is a member of APS, MRS, SPIE, TMS, and Tau Beta Pi.

Miroslav Micovic received the B.Sc. degree in physics from University of Ljubljana, Ljubljana, Slovenija in 1989.

From 1990 to 1992, he was Research Assistant at Laboratorio TASC, Trieste, Italy, working on III-V Molecular Beam Epitaxy. From 1992 to 1993 he was consultant at AT&T Bell Laboratories, Murray Hill, NJ, investigating the use of carbon doping for the growth of structures for fabrication of semiconductor laser diodes and heterojunction bipolar transistors by solid source MBE. In 1993, enrolled in the Ph.D. program in electrical engineering at The Pennsylvania State University where he is involved in the work of the MBE group at the Electronic Materials and Processing Research Laboratory. Currently investigating the use of halogens in solid source MBE.

David L. Miller (M'88) received the A.B. degree in physics from Whitman College in 1966 and the M.S. and Ph.D. degrees in physics from the University of Illinois, Urbana in 1967 and 1973, respectively.

He is Professor in the Department of Electrical Engineering at The Pennsylvania State University, University Park, PA, and member of the Center for Electronic Materials and Processing. From 1977 to 1988 he was employed in semiconductor research and management at the Rockwell International Science Center, Thousand Oaks, CA. His research interests include the growth and characterization of III-V materials, high-speed electronic and optoelectronic devices, and molecular beam epitaxy.